

This is an Open Access document downloaded from ORCA, Cardiff University's institutional repository: <https://orca.cardiff.ac.uk/id/eprint/121055/>

This is the author's version of a work that was submitted to / accepted for publication.

Citation for final published version:

Domènech, Guillem, Fan, Xuanmei, Scaringi, Gianvito, van Asch, Theo W.J., Xu, Qiang, Huang, Runqiu and Hales, Tristram C. 2019. Modelling the role of material depletion, grain coarsening and revegetation in debris flow occurrences after the 2008 Wenchuan earthquake. *Engineering Geology* 250 , pp. 34-44. 10.1016/j.enggeo.2019.01.010

Publishers page: <http://dx.doi.org/10.1016/j.enggeo.2019.01.010>

Please note:

Changes made as a result of publishing processes such as copy-editing, formatting and page numbers may not be reflected in this version. For the definitive version of this publication, please refer to the published source. You are advised to consult the publisher's version if you wish to cite this paper.

This version is being made available in accordance with publisher policies. See <http://orca.cf.ac.uk/policies.html> for usage policies. Copyright and moral rights for publications made available in ORCA are retained by the copyright holders.



**Modelling the role of material depletion, grain coarsening and revegetation
in debris flow occurrences after the 2008 Wenchuan earthquake**

Guillem Domènech^a, Xuanmei Fan^{a,*}, Gianvito Scaringi^a, Theo W.J. van Asch^{a,b}, Qiang Xu^a,
Runqiu Huang^a, Tristram C. Hales^c

^a State Key Laboratory of Geohazard Prevention and Geoenvironment Protection, Chengdu
University of Technology, Chengdu, 610059, People's Republic of China

^b Faculty of Geosciences, Utrecht University, Heidelberglaan 2, 3584 CS, The Netherlands

^c School of Earth and Ocean Sciences, Sustainable Places Research Institute,
Cardiff University, Cardiff, CF10 3AT, United Kingdom

* Corresponding to: Prof. Xuanmei Fan (fxm_cdut@qq.com)

Abstract

A large amount of debris was generated by the co-seismic mass wasting associated with the 2008 M_w 7.9 Wenchuan earthquake. The abundance of this loose material along the slopes caused more frequent debris flows, triggered by less intense and/or shorter rainfalls. However, both the triggering rainfall and the debris flow frequency seem to have normalised progressively during the past decade. Although changes of rainfall thresholds for post-seismic debris flows were recorded after several major earthquakes, the factors controlling these changes remain poorly constrained. With the aid of a virtual experiment, we investigate the roles of material depletion, grain coarsening and revegetation of the co-seismic debris on the propagation and deposition of debris flows initiated by runoff, as well as their influence on the triggering rainfall thresholds. We employ a Geographic Information System (GIS)-based simulation of debris flow initiation by runoff erosion, which we first calibrate on the 14th August 2010 Hongchun gully event that occurred near the Wenchuan earthquake epicentre. We obtain, by investigating each of the aforementioned processes, changing critical rainfall intensity-duration thresholds for given debris flow runout distances. Grain coarsening appears to play a major role, which is consistent with published laboratory experiments, while material depletion and revegetation do not seem able to account alone for the actual quick decay of debris flow frequency. While the virtual experiment has proven useful in identifying the first-order controls on this decay, model improvements and verification over multiple catchments are needed to make the results useful in hazard assessments.

Keywords: debris flow evolution; material depletion; grain coarsening; revegetation; rainfall thresholds; Wenchuan earthquake

1. Introduction

The 2008 M_w 7.9 Wenchuan earthquake (Sichuan, China) triggered a great number of co-seismic landslides (Fan et al., 2018b; Huang and Fan, 2013), many of which were later remobilised into catastrophic debris flows triggered by rainfalls (Tang et al., 2011). A sharp increase of the frequency of debris flows was observed soon after the earthquake (Domènech et al., 2018; Fan et al., 2018b, 2018a, 2018c; Huang and Fan, 2013) in combination with a reduction of the debris flow-triggering rainfall thresholds (Guo et al., 2016b, 2016a). However, debris flows frequency and rainfall thresholds in the Wenchuan earthquake-struck area seem to have normalised already (Zhang and Zhang, 2017), following a decay similar to that observed in other mountainous regions hit by strong earthquakes (Hovius et al., 2011; Marc et al., 2015).

Kean et al. (2013) grouped the debris flows initiated by runoff into two categories: mass failure of the channel sediment by sliding along a discrete failure plane and grain-by-grain bulking by hydrodynamic forces (runoff erosion). Investigations carried out so far, and discussed in the following paragraphs, suggest that the evolution of debris flow activity is strongly controlled by: (1) the depletion of the erodible material by successive landsliding (e.g., Saito et al., 2014; Zhang and Zhang, 2017); (2) grain coarsening, that increases the hydraulic conductivity, favouring water drainage and limiting bed entrainment (e.g., Abancó and Hürlimann, 2014; Cuomo et al., 2016; Hu et al., 2017; Zhang and Zhang, 2017) and (3) revegetation, that reduces the soil erodibility, increases its shear strength and its infiltration capacity (e.g., Hales, 2018; Reubens et al., 2007; Schwarz et al., 2010; Zhu and Zhang, 2016).

Depletion of the hillslope material is a primary cause of decreasing debris flow volumes under a given hydrological forcing (Saito et al., 2014), which has been observed in the Wenchuan earthquake-affected area also through the decreasing of runout distances and

deposition widths over time (Zhang and Zhang, 2017), and has been reproduced by numerical simulations of debris flows (van Asch et al., 2014). These led the authors to conclude that rainfall thresholds increase after successive rain events as a result of a depletion of erodible material in the channels. Nevertheless, the frequency of debris flows decreased significantly in the Wenchuan earthquake-affected area even though most of the co-seismic debris is still in place (Domènech et al., 2018; Fan et al., 2018c).

The preferential washing away of the finest particles and the consequent progressive coarsening of the debris flow material observed in the Wenchuan earthquake-affected area (Chen et al., 2014) has been linked with the decreasing runout and deposition distances (Zhang et al., 2013; Zhang and Zhang, 2017) as soil erodibility decreased progressively (Chang et al., 2011). Experiments on artificial instrumented slopes demonstrated the controlling role of soil grading and, particularly, of that of the smallest particles in the initiation and kinematics of flow-like landslides (Hu et al., 2017; Wang and Sassa, 2003, 2001). Hu et al. (2017) found the internal erosion of the smallest soil fraction and its effect on the hydraulic conductivity (k_s , m/s) to be a critical factor in the nucleation and development of instability that leads to flow-like landslides in loose granular assemblies.

Field investigations (Julian and Torres, 2006; Zhu and Zhang, 2016), laboratory tests (Mamo and Bubenzer, 2001) and numerical simulations (Shen et al., 2017) have been conducted to analyse the effect of revegetation on soil erosion and slope stability. A significant increase of the soil shear strength has been observed (e.g., Veylon et al., 2015; Waldron and Dakkessian, 1981; Wu, 2013;), that leads to an increased stability. Shen et al. (2017) modelled the effects of revegetation on hillslope erosion adopting the approach described by Zhu and Zhang (2016). They linked the changes of critical erosive shear stress (τ_c , kPa) and coefficient of erodibility (k_d , kPa) with the revegetation using the Root Mass Density (RMD , kg/m³). This

quantity describes the ratio between the mass of dry roots and the mass of the root-permeated dry soil:

$$RMD = \frac{M_R}{M_S} \quad (1)$$

where M_R (kg) is the dry mass of roots and M_S (kg) is the dry mass of the entire sample.

While independent studies investigated the effects of the aforementioned processes individually, a comparative quantification of their role is lacking. By means of a virtual experiment, here we analyse the role of material depletion, grain coarsening and revegetation of the co-seismic debris at catchment scale. We compare their influence on the propagation and deposition of debris flows, initiated by runoff, as well as on the rainfall thresholds. Even though we use a site-specific setting as our baseline, we follow the input of [Weiler and McDonnell \(2004, 2006\)](#), who proposed the use of virtual experiments for a systematic examination of the first-order controls on complex and coupled hydro-mechanical processes. Virtual experiments, defined as *numerical experiments with a model driven by collective field intelligence*, can allow to assess the main and essential process constraints, whereas the irregular bedrock and surface topography and the spatial variability in soil properties make the isolation of causes and effects challenging in field studies ([Weiler and McDonnell, 2006](#)). A number of physically-based models have been proposed to simulate rainfall-induced soil erosion, transportation and deposition ([Cuomo et al., 2015](#)): the Water Erosion Prediction Project (WEPP) model ([Nearing et al., 1989](#)), the Limburg Soil Erosion Model (LISEM; [De Roo, 1996](#)), the EUROpean Soil Erosion Model (EUROSEM; [Morgan et al., 1998](#)), and the Erosion-Deposition Debris flow Analysis (EDDA 1.0) model ([Chen and Zhang, 2015](#)), among others. In this parametric study, aimed at identifying the first-order process constraints, a modified version of [van Asch et al. \(2014\)](#)'s model, implemented in PCRaster GIS environment ([Karssenberget al., 2001](#)), has been chosen for its simplicity and ease to use and modify. An early version of this model was

applied by [van Asch et al. \(2014\)](#) to our study area, proving itself useful in reproducing the main features of the actual debris flow event, on which it was calibrated. In this work, we first re-calibrated the model on the 14th August 2010 debris flow event that occurred at Hongchun gully (Sichuan, China). Then, relations from the literature that characterise the three aforementioned processes are integrated into the model and used to simulate possible scenarios of evolutions of debris flow activity. The results are then discussed in terms of debris flow volumes and runout and of changes of the critical rainfall thresholds.

2. Study area

The Hongchun gully (103°30'21" E, 31°4'12" N) is a left-bank tributary of the upper course of the River Min (Minjiang). Its outlet is located just upstream of the urban centre of the town of Yingxiu, very close to the epicentre of the 2008 Wenchuan earthquake. ([Fig. 1a](#)). It subtends a catchment area of 5.35 km², with elevations ranging from 880 to 1700 m a.s.l. ([Fig. 1b](#)). The bedrock is mainly composed of deeply fractured and highly weathered granitic rock, Sinian pyroclastic rock, Carboniferous limestone and Triassic sandstone ([Tang et al., 2011](#)). The volume of co-seismic debris generated by the co-seismic mass wasting in the catchment can be quantified in about $9.3 \times 10^6 \text{ m}^3$.

On 14th August 2010 at 03:00 h, a large debris flow occurred in the gully ([Fig. 1c](#)). It was preceded by 162.1 mm precipitation accumulated during 33 h (from 17:00 h on 12th August to 02:00 h on 14th August, local time). During the hour prior to the debris flow initiation, a rainfall intensity of 16.4 mm/h was recorded ([Fig. 1d](#)). The debris flow initiated in the erosive rills on the co-seismic deposits in the upper reaches of the catchment, due to the overland flow that progressively eroded the deposits and transported the debris into the gully ([Tang et al., 2011](#)). Eyewitnesses indicated that the largest surge moved between 03:00 h and 04:30 h. It resulted in a volume of about $7.11 \times 10^5 \text{ m}^3$ ([Tang et al., 2011](#)) forming a deposition fan at the

outlet of the catchment, with about $4 \times 10^5 \text{ m}^3$ reaching the River Min (Li et al., 2013), obstructing its course and thus flooding the newly reconstructed Yingxiu town and causing dozens of victims.

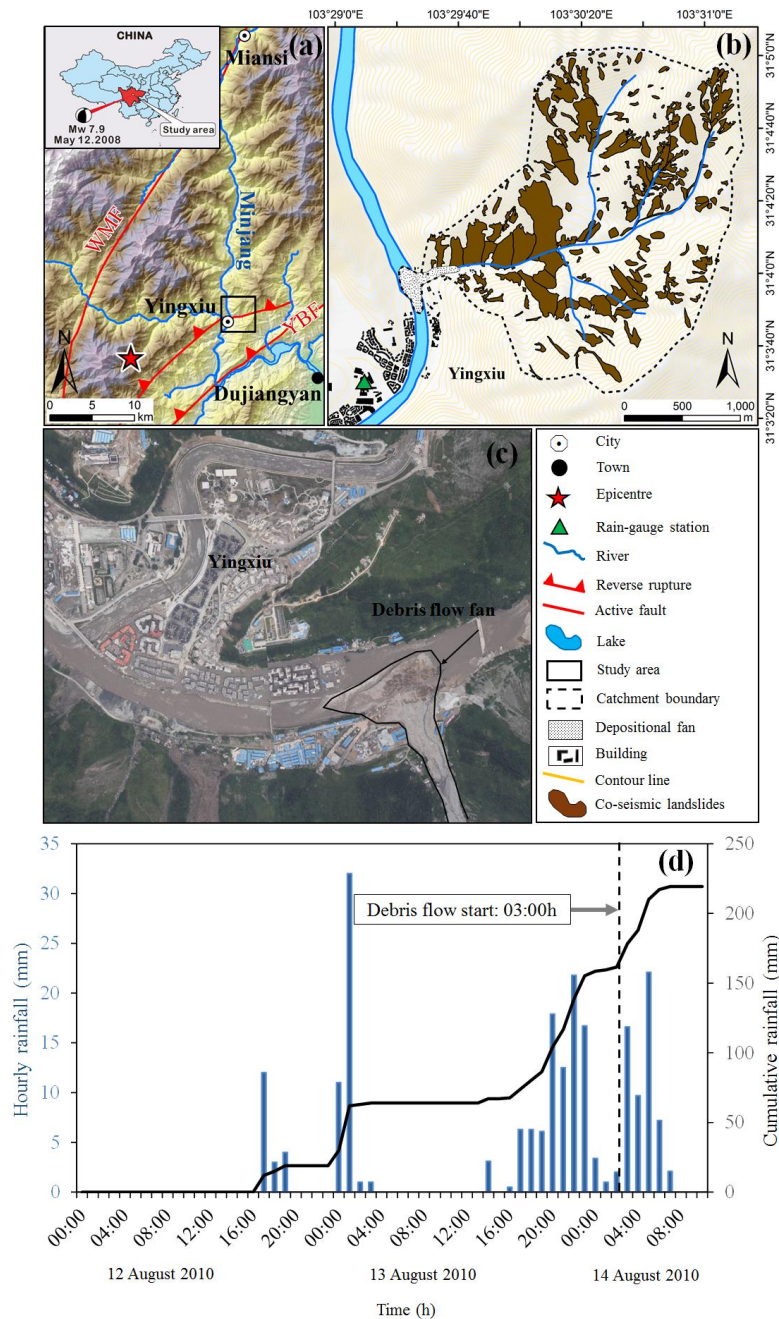


Figure 1. Study area and triggering rainfall. a) General view of the epicentral area of the Wenchuan earthquake and its location in Sichuan, China. The study area is indicated by a black square; b) map of the Hongchun gully displaying the co-seismic landslide deposits; c) aerial

photo taken on 15th August 2010 showing the depositional fan of the 14th August 2010 debris flow; d) hourly and cumulative rainfall between 12th and 14th August 2010 recorded in Yingxiu.

3. Data and methods

3.1 Topography, co-seismic deposits and rainfall data

The model runs on a 10 m resolution Digital Elevation Model (DEM). Information on the landslide deposits was obtained from a detailed inventory compiled through polygon-based visual interpretation of high-resolution satellite images and aerial photographs (Fig. 1b) (Domènech et al., 2018; Fan et al., 2018c). A total of 202 co-seismic landslides were identified in the study area. The average depth of the deposits of co-seismic debris (d , m) was estimated for each mapped area using the empirical relationship proposed by Tang et al. (2011), calibrated through the analysis of 62 deposits of various size in Hongchun gully and in the nearby Shaofang gully:

$$d = 1.2 \ln S_L - 5.6 \quad (2)$$

where S_L (m²) is the individual landslide area. d is thus estimated to range from 0.4 to 8.6 m, with an average value of 4 m. It results in a range of volumes of the individual deposits between 59 m³ and over 1.2x10⁶ m³. The total volume results approximately equal to 9,1x10⁶ m³.

Rainfall data with hourly resolution were retrieved from a rain gauge installed in Yingxiu. It is located at 800 m a.s.l., 600 m from the Hongchun gully outlet (Fig. 1d).

3.2 Model description

In the model, erosion by runoff occurs when the bed shear stress (τ , kPa) is larger than the critical erosive shear stress at initiation of soil erosion (τ_c , kPa), and the volumetric

concentration of solids in the debris flow (C_v) is smaller than an equilibrium value ($C_{v\infty}$). We use the expression for the latter as proposed by [Takahashi et al. \(1992\)](#):

$$C_{v\infty} = \frac{\rho_w \tan \theta}{(\rho_s - \rho_w)(\tan \phi_{bed} - \tan \theta)} \quad (3)$$

where ρ_w (kg/m³) is the density of water, ρ_s (kg/m³) is the density of the solids, ϕ_{bed} (°) is the internal friction angle of the bed material and θ (°) is the slope angle. The erosion rate can be expressed as ([Takahashi et al., 1992](#)):

$$i = \delta_e \frac{a_c}{d_L} U = \delta_e \frac{C_{v\infty} - C_v}{C_{v*} - C_{v\infty}} \frac{q_t}{d_L} \quad (4)$$

where δ_e is a non-dimensional coefficient of erosion rate that has been obtained through back-analysis, a_c (m) is the depth within the sediment layer where $\tau_c = \tau$, d_L is assumed to be the same as that of the source material of the debris flow, U (m/s) is the sectional mean velocity of the flow, C_{v*} is the volumetric fraction of solids in the erodible bed and q_t (m²/s) is the total discharge of the sum of sediment and water per unit width expressed as ([van Asch et al., 2014](#)):

$$q_t = (H_s + H_w)V = (H_s + h_r T_s)V \quad (5)$$

where H_s (m) is the equivalent height of solids, H_w (m) is the equivalent height of water, V (m/s) is the flow velocity, and T_s (s) is the time step duration. h_r is calculated using a simple-lumped infiltration model that ignores the effect of the initial moisture content and sorptivity of the soil ([van Asch et al., 2014](#)):

$$h_r = (r - k_s) \quad (6)$$

where r (m/s) is the rain intensity.

The solid materials of a debris flow begin to deposit when V is smaller than a critical flow velocity (V_e , m/s), and at the same time C_v is larger than $C_{v\infty}$. We use the V_e proposed by [Takahashi et al. \(1992\)](#):

$$V_e = \frac{2}{5d_L} \left(\frac{g \sin \theta_e \rho}{0.02 \rho_s} \right)^{0.5} \lambda^{-1} h^{1.5} \quad (7)$$

where g (m/s²) is the gravity acceleration, h (m) is the flow height, θ_e (°) is the flattest slope on which a debris flow that comes down through the change in slope does not stop, and ρ (kg/m³) is the bulk density of the debris flow. θ_e and ρ are defined as:

$$\theta_e = \text{atan} \left(\frac{C_v(\rho_s - \rho_w) \tan \phi_{bed}}{C_v(\rho_s - \rho_w) + \rho_w} \right) \quad (8)$$

$$\rho = C_v(\rho_s - \rho_w) + \rho_w \quad (9)$$

Moreover:

$$\lambda^{-1} = \left(\frac{C_{v*}}{C_v} \right)^{1/3} - 1 \quad (10)$$

The deposition rate (i , m/s) can be expressed as ([Takahashi et al., 1992](#)):

$$i = \delta_d \left(1 - \frac{V}{pV_e} \right) \frac{C_{v\infty} - C_v}{C_{v*}} V \quad (11)$$

where δ_d is a non-dimensional coefficient of deposition rate obtained through back-analysis and $p(<1)$ is a non-dimensional coefficient to describe the initiation of the depositing process. A value of 0.67 for the latter is recommended by [Takahashi et al. \(1992\)](#).

Assuming turbulent flow conditions, which seem likely in steep and rough channels ([Montgomery and Buffington, 1997](#)), V is calculated using the Manning's equation when C_v is below an arbitrarily chosen limit of 0.4 ([van Asch et al., 2014](#)).

$$V = \frac{h^{2/3} \sin \theta^{1/2}}{n} \quad (12)$$

where n ($\text{m}^{1/3}/\text{s}$) is the Manning's number equal to 0.04 (van Asch et al., 2014). For $C_v > 0.4$ (van Asch et al., 2014), a simple equation of motion is used:

$$\frac{\partial v}{\partial t} = g(\sin\theta \cos\theta - k \tan\theta - S_f) \quad (13)$$

where k is the lateral pressure coefficient (taken equal to 1; van Asch et al. (2014), and S_f is a resistant factor depending on the rheology of the flow:

$$S_f = \cos^2\theta \tan\varphi' + \frac{1}{\rho gh} \left(\frac{3}{2} \tau_c + \frac{3\mu}{h} V \right) \quad (14)$$

where φ' ($^\circ$) is the apparent friction angle of the flow for a certain pore water pressure, and μ ($\text{kPa}\cdot\text{s}$) is its dynamic viscosity.

3.3 Model calibration

The model simulates the initiation of debris flow by surface runoff. It is an improved version of the model written by van Asch et al. (2014). δ_e , and k_s were calibrated by back analysis to match the volume and shape (by visual estimation and matching degree (Fan et al., 2018a) of the 14th August 2010 debris flow fan deposit at the outlet of the catchment, and the time that the debris flow reached the River Min (as reported in Tang et al., 2011). In the model, the River Min was assumed to be flowing below 895 m a.s.l. (Ouyang et al., 2015).

3.4 Effects of material depletion, grain coarsening and revegetation

In order to analyse the effect of the decreasing availability of erodible material due to successive debris flows events in the catchment, the parameters calibrated through back analysis were kept unchanged, while the output of one simulation was used as the input for the next simulation. For simplicity, and to eliminate the effect of rainfall variability, we kept using the 14th August rainfall pattern in all simulations. We repeated the simulations until the runoff-

eroded material was insufficient to generate a debris flow that reached the outlet of the catchment.

Grain coarsening was accounted for in the model by increasing the mean diameter of the solid grains (d_{50}) and, consequently, the k_s of the granular assembly. As a matter of fact, research carried out in the Wenchuan earthquake-affected area (Chen et al., 2014; Zhang et al., 2014; Zhang and Zhang, 2017) indicates that actual successive debris flows events were characterised by increasingly coarser material due to the preferential loss of the finest particles. Evidence of this was provided experimentally by Hu et al. (2017) on artificial slopes. For loose granular slopes prepared at a given relative density, the authors evaluated significant changes of k_s and d_{50} in dependence of the progressing erosion of the granular fraction that can be transported by seepage through the soil pores. In this research, the model calibration was performed using d_{50} resulting from the highest percentage of small particles (dimension smaller than 0.5 mm). For the successive simulations, d_{50} was increased to account for the decreasing proportion of small erodible particles, until they were completely washed away. In parallel, k_s increases due to the increasing pore size and pore network connectivity. To reproduce this, we associated to each d_{50} a value of k_s following the trend observed by Hu et al. (2018, 2017). The different values of d_{50} and k_s were later compared and discussed with those obtained from other studies performed in the study area. For all simulations, we used each time the input layer containing the full amount of co-seismic material.

Regarding the revegetation effect, Zhu and Zhang (2016) simulated the process by increasing τ_c , and decreasing k_d :

$$i = k_d(\tau - \tau_c) \quad (15)$$

Changes of τ_c are introduced in eq. 14 accordingly.

To quantify the effect of the revegetation, we used the results obtained by Shen et al. (2017) in the Xiaojiagou Ravine, 5 km away from our study area. The authors quantified the revegetation on a hillslope in the years 2010, 2013 and 2015 using the *RMD* (Zhu and Zhang, 2016). Then, they related the changes of *RMD* with those of τ_c and k_d using the empirical relationships proposed by Zhang et al. (2013) and Zhu and Zhang (2016), and considering the 2010 condition as that of a bare slope:

$$\tau_c^{coeff} = \frac{\tau_{c \text{ for a given } RMD}}{\tau_{c \text{ for a bare slope}}} \quad (16)$$

$$k_d^{coeff} = \frac{k_{d \text{ for a given } RMD}}{k_{d \text{ for a bare slope}}} \quad (17)$$

Shen et al. (2017) found an increase of *RMD* by 0.16% in 2013 (mid-level revegetation) and of 0.4% in 2015 (high-level revegetation). For 2013, this was translated into an increase of τ_c by 80% and a decrease of k_d by 40%. In 2015, the increment of τ_c was of 140% and a decrease of k_d by 60% compared to 2010.

3.5 Assessment of the changing rainfall thresholds

A parametric analysis was conducted to analyse the influence of material depletion, grain coarsening and revegetation on the critical rainfall in terms of intensity-duration (ID) thresholds. Taking the result of the calibrated model as the initial condition, the evolution of the ID curves was analysed, separately, for each process. For instance, the ID curves for the years 2010, 2013 and 2015 were calculated to analyse the effect of the revegetation. Each curve refers to the amount of rainfall, within a given period of time, necessary to generate a debris flow by runoff erosion that reaches the outlet of the gully.

4. Results

4.1 Model calibration

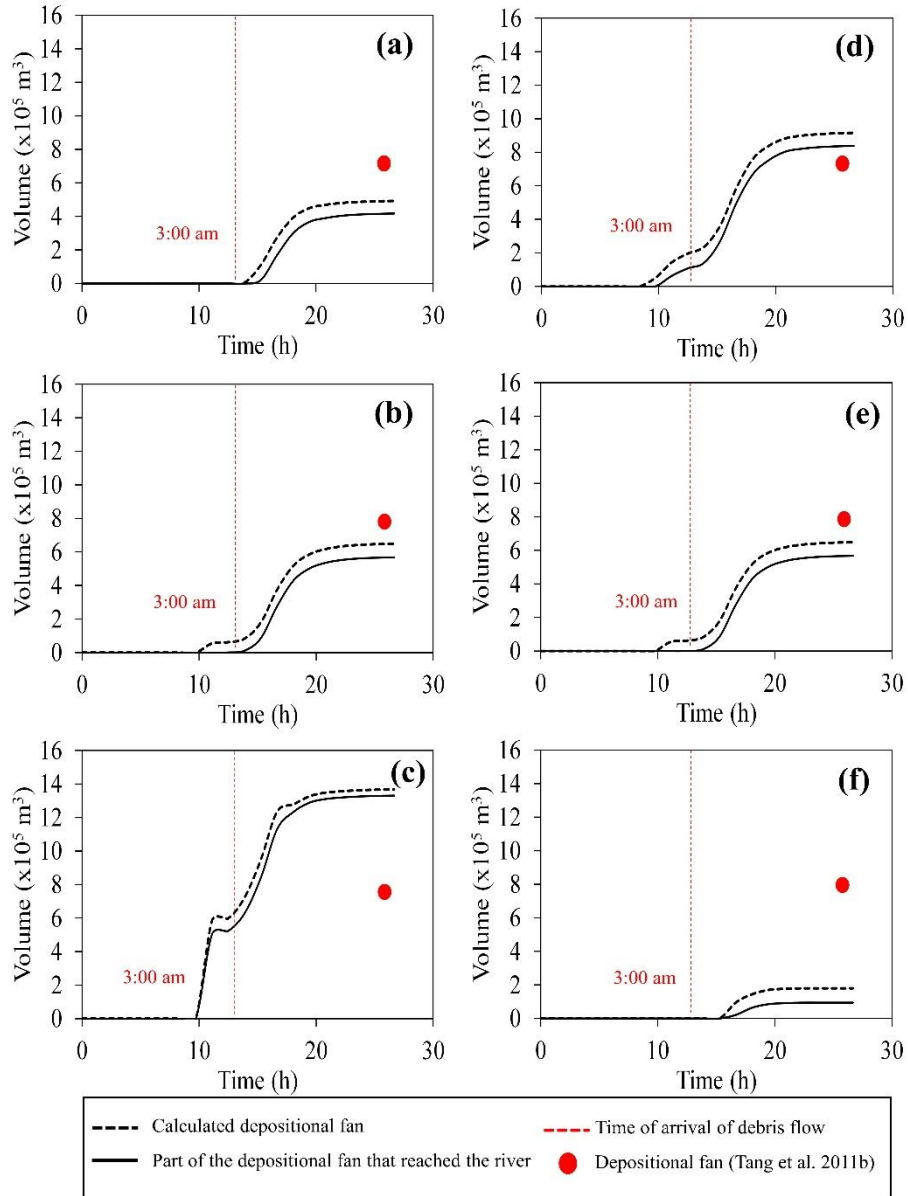
The best-fit model parameters used during the calibration at Hongchun gully are listed in [Table 1](#). d_{50} , ρ_s , C_{v*} , ϕ_{bed} , τ_c , δ_d , μ and n have been taken from the literature as specified below. On the other hand, δ_e , k_s were calibrated by back analysis. Assuming a high proportion of small particle content in the co-seismic deposits of the Wenchuan earthquake (between 2% and 26% ([Wang et al., 2017](#)), the grain size distribution obtained by [Hu et al. \(2017\)](#) in a co-seismic deposit from Wenjia gully, which range from 0.1 to 22% of small particle content, has been used. Therefore, a d_{50} of 1.9 mm of the source material that corresponds to the maximum percentage of small particle contents (22%), i.e. the co-seismic situation before the erosion started, was chosen. It is of the same order of magnitude as the d_{50} obtained by [Zhang et al. \(2014\)](#) in the 24th June 2008 debris flow events occurred in Pubugou Ravine (0.7 mm), which is approximately 5 km away from Hongchun gully with a similar geology mainly composed of igneous rocks such as granodiorite and diorite and quaternary deposits. C_{v*} and ϕ_{bed} were chosen equal to 0.65 and 35°, respectively. The first one is based on the flume experiments carried out by [Takahashi et al. \(1992\)](#) and later used by [Chen and Zhang \(2015\)](#) and [Shen et al. \(2017\)](#) during their simulations. [Shen et al. \(2017\)](#) obtained the ϕ_{bed} from field and laboratory tests carried out in the Xiaojiagou Ravine, located beside Pubugou Ravine, at 6.0 km from Hongchun gully and composed of igneous rocks as well. δ_d was chosen based on the results obtained by [van Asch et al. \(2014\)](#) which is equal to 0.0001. Both τ_c and μ are based on the results of simulations carried out in Hongchun gully ([Ouyang et al., 2015](#)) and Shuida gully ([van Asch et al., 2014](#)), with 1 kPa and 1 kPa-s. Regarding δ_e and k_s , a sensitivity analysis has been carried out to check their influence ([Fig. 2](#)). Results for three different values of δ_e (0.01, 0.1 and 1) and k_s (0.0015 m/h, 0.003 m/h and 0.006 m/h) are presented in [Fig. 2a-c](#) and [Fig. 2d-f](#), respectively. It can be seen as the amount of debris flows generated and its velocity of the

flow increases for higher values of δ_e . Conversely, for higher values of k_s the generated volume of debris flow and its velocity decreases. Considering the volume of debris flow at the depositional fan (red dot), calculated by Tang et al. (2011) from field investigations, and the time of arrival of the main event at the river (dashed red line), described also by Tang et al. (2011), the best fit has been found to be with $\delta_e = 0.1$ and $k_s = 0.003$ m/h.

Table 1. Parameters used during the calibration of the 14th August 2010 debris flow event in Hongchun gully. d_{50} , ρ_s , C_{v*} , ϕ_{bed} , τ_c , δ_d , μ and n have been taken from the literature. On the other hand, δ_e , k_s were calibrated by back analysis.

| d_{50} (mm) | ρ_w (kg/m ³) | ρ_s (kg/m ³) | C_{v*} | ϕ_{bed} (°) | τ_c (kPa) | δ_e | δ_d | k_s (m/h) | μ (kPa·s) | n |
|------------------|----------------------------------|----------------------------------|----------|---------------------|-------------------|------------|------------|----------------|------------------|------|
| 1.9 | 1000 | 2600 | 0.65 | 35 | 1 | 0.1 | 0.0001 | 0.003 | 1 | 0.04 |

d_{50} = mean grain size; ρ_w = density of water; ρ_s = density of solid particles; C_{v*} = volume fraction of solids in the erodible bed; ϕ_{bed} = friction angle of soil; τ_c = yield strength; δ_e = coefficient of erosion rate; k_s = soil infiltration capacity; μ = dynamic viscosity; n = Manning's number



297

298 **Figure 2.** Temporal evolution of the calculated volume at the depositional fan (dashed black
 299 line) and part of the deposit that reached the river (black line) for the 14th August 2010 event
 300 in Hongchun gully using PCRaster. The debris flow simulation started on 13th August 2010 at
 301 14:00 h and lasted for 24 h. Coefficient of erosion rate $\delta_e = 0.01$ (a), $\delta_e = 0.1$ (b), $\delta_e = 1$ (c).
 302 Soil infiltration capacity $k_s = 0.0015$ (d), $k_s = 0.003$ (e), $k_s = 0.006$ (f). The red dot indicates
 303 the volume estimated by Tang et al. (2011) in the depositional fan. The time of arrival of the
 304 main debris flow is indicated by a dashed red line (03:00 am, Tang et al., 2011).

305

306 The results of the calibrated model are presented in Fig. 3. The debris flow event
307 simulation started from 13th August 2010 at 14:00 h and lasted for 24 h. The code is able to
308 reproduce the deposition of the debris flow, mostly accumulated along the main channel and
309 at the outlet of the catchment, blocking the River Min (Fig. 3a). The simulated debris flow fan
310 has an area of 113,280 m², which is larger than the 75,740 m² mapped from observations made
311 by Tang et al. (2011) (depositional fan in Fig. 3a) representing a matching degree (Fan et al.,
312 2018a) of 0.67. This mismatch could be partly due to the fact that the mapping has been done
313 using an aerial image that prevents the identification of some parts of the fan submerged into
314 the river and that the picture was taken one day after the event, being some material from the
315 fan already eroded. Actually, the part of the simulated deposit that does not match with the
316 field mapping (Tang et al., 2011) is the one located downstream with a maximum flow height
317 between 1 and 4 m. With this height, the material flooded into the River Min is submerged and
318 thus the area of the fan mapped in the field is underestimated. On the other hand, it also could
319 be due to the fact that the model is not able to reproduce, exactly, the spreading of the
320 depositional fan as it was already observed by van Asch et al. (2014). The simulated debris
321 flow reached the river 14 hours after the initiation of the simulation, i.e., around 14th August
322 2010 at 04:00 h (Fig. 3b). It represents one hour of delay regarding the observations made by
323 the eyewitness who indicated that the most important debris flows started around 03:00 h (Tang
324 et al., 2011). This delay could be due to the failure of a debris dam upstream in the Hongchun
325 gully, that the code is not able to simulate, and which increased the flow discharge, the
326 transported debris volume (Tang et al., 2011) and consequently, its velocity and capacity of
327 erosion. This effect was already observed during the calibration of the model when increasing
328 the non-dimensional coefficient of erosion rate (Fig. 2a-c). The total volume simulated on the
329 depositional fan is about $6.5 \times 10^5 \text{ m}^3$ from which, about $5.7 \times 10^5 \text{ m}^3$ reached the river with a

maximum thickness of 17 m (Fig. 3b). There is an underestimation of the material deposited in the fan of about 9% with respect to the one mapped by Tang et al. (2011), i.e. $7.11 \times 10^5 \text{ m}^3$. The difference could be a result of other processes observed during the debris flow propagation. As a matter of fact, entrainment, collapses of the sidewalls, channel damming and breaching can enhance the debris flow volume (Chen et al., 2006; Hu et al., 2016) but cannot be accounted for in our simplified model. Nevertheless, the 9% of difference indicates that they were not very relevant in this case and our model is able to reproduce the amount of material transported at the depositional fan satisfactorily.

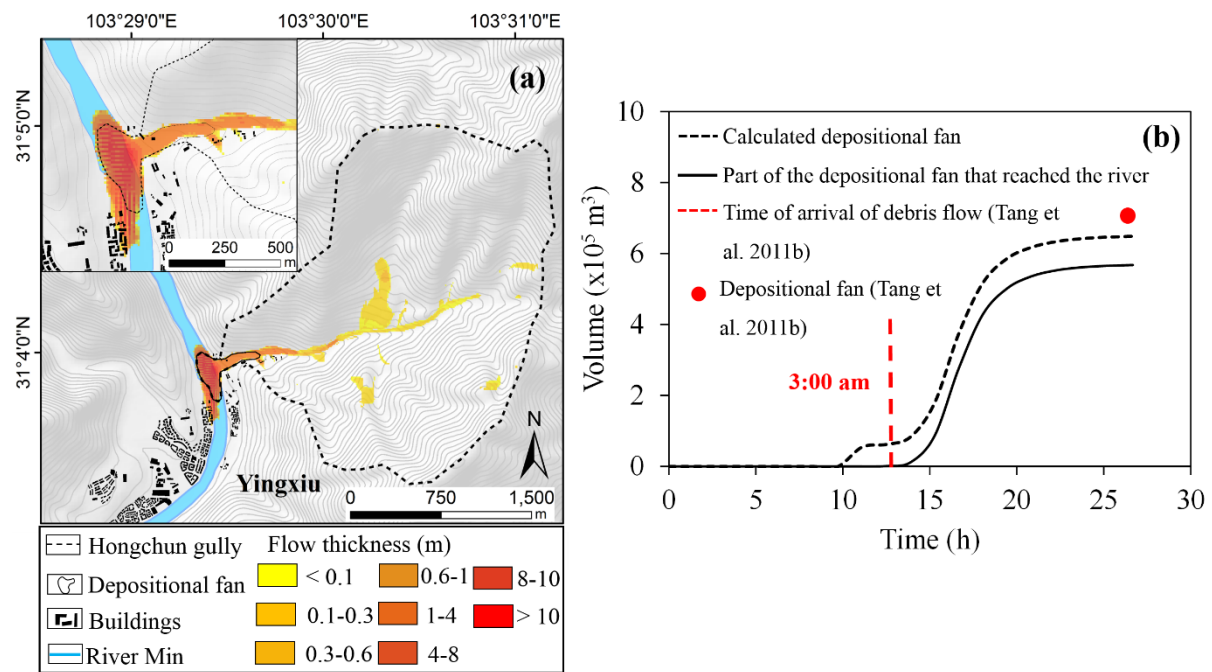


Figure 3. Best simulation of the 14th August 2010 debris flow event at Hongchun gully using PCRaster: (a) General view of the calculated flow height and zoom in of the depositional fan at the outlet of the catchment. Parameters used in the simulation are described in Table 1. (b) Temporal evolution of the calculated volume at the depositional fan (dashed black line) and part of the deposit that reached the river (black line). The red dot indicates the volume (Tang et al., 2011) in the depositional fan. The time of arrival of the main debris flows at the river is indicated with a dashed red line (3:00 am, Tang et al., 2011).

4.2 Effects of material depletion, grain coarsening and revegetation on the debris flow volumes

Regarding the material depletion, the volumes of debris flow triggered in 5 successive simulations, accounting for the erosion of the co-seismic deposits after each simulation, are presented in [Fig. 4a](#). The largest events were generated during the first three simulations, where 648,431 m³, 631,560 m³ and 609,605 m³ were deposited at the depositional fan, consecutively. Then, for the following two simulations, the eroded material decreased dramatically until no erosion occurred during the fifth simulation. In general, most of the erosion was given in the main channels where a larger amount of accumulated water is present ([Fig. 5](#)). The amount of material evacuated from the catchment after four simulations represents only the 25% of the total co-seismic landslides triggered by the earthquake ([Table 2](#)). Therefore, there is still a 75% of material remaining along the hillslopes that is not mobilized as debris flow under the chosen input rainfall event. In this case, since the erosion is mostly given in the main channels, once the material has been washed away, the runoff in the remaining deposits is not enough to generate a debris flow. However, in other settings (e.g. [Zhang and Zhang, 2017](#)), it is likely that the erosion of the debris deposits toes that are located in steep slopes induce an instability in the whole deposit, providing additional material to the main channel that could enlarge the final total volume or contribute to the next simulation.

Table 2. Results obtained during the simulation of the material depletion. Each simulation was computed using the remaining material in the loose deposits that was not eroded in the previous one. The debris flow at the depositional fan and the accumulated loose material evacuated from the catchment after each simulation are listed.

| Simulation number | Volume of depositional fan (m ³) | Accumulated material evacuated from the catchment (%) |
|-------------------|--|---|
| 1 | 648,431 | 7 |
| 2 | 631,560 | 14 |
| 3 | 609,605 | 20 |
| 4 | 438,108 | 25 |
| 5 | 0 | 25 |

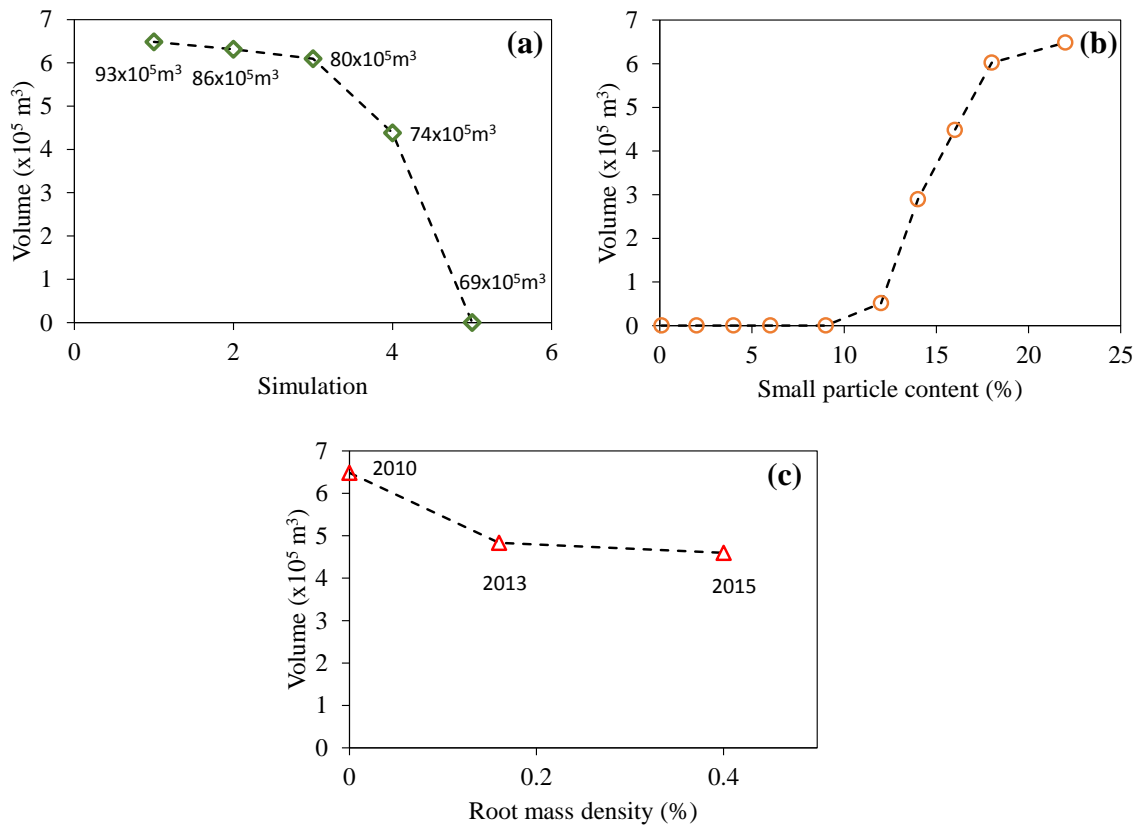


Figure 4. Evolution of the simulated debris flow volumes that reach the outlet of Hongchun gully for each process: a) material depletion after each simulation (Table 2). The available erodible material before each simulation is represented; b) grain coarsening in terms of small particles content (Table 3); c) revegetation for a given RMD (Table 4). The corresponding year for each RMD, according to Shen et al. (2017), is also shown.

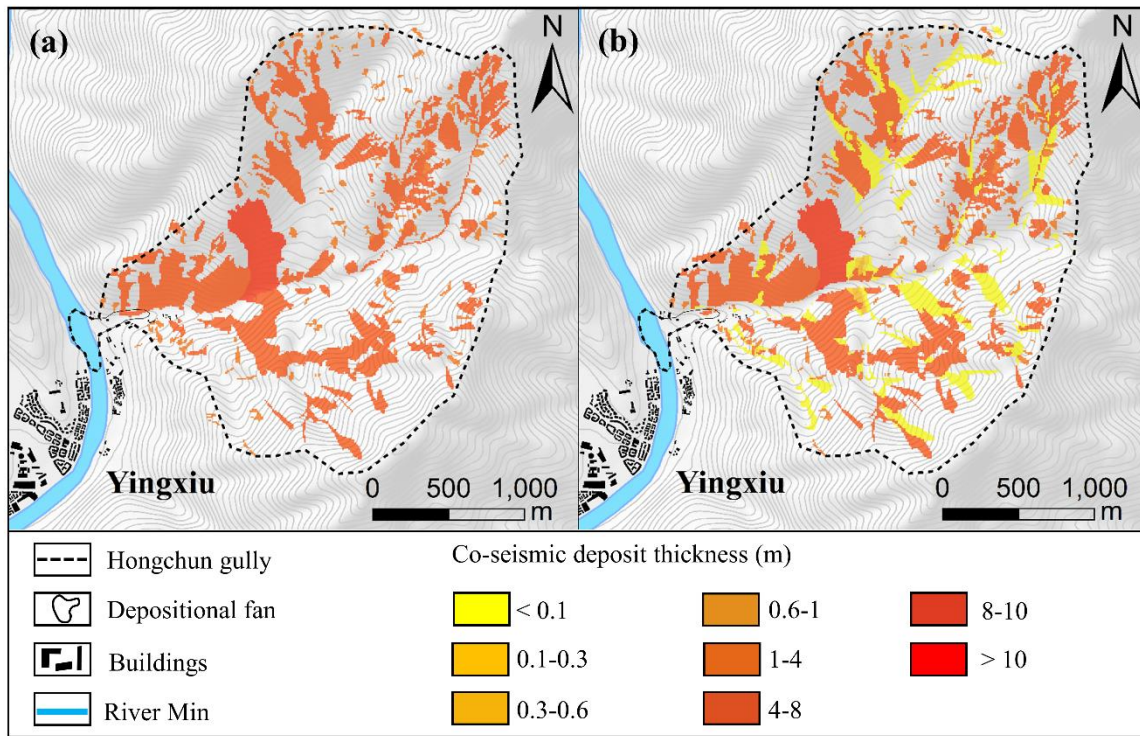


Figure 5. Simulated evolution of the co-seismic deposits due to material depletion. Initial thickness (in meters) of the co-seismic landslide deposits before simulating the 14th August 2010 debris flow event in Hongchun gully (a). Non-eroded material after four simulations using the calibrated parameters in PCRaster (Table 1) and using the remaining material of the previous simulations as input for the following one (b).

The influence of the grain coarsening is shown in Fig. 4b. With the decreasing of the small particles content (dimension smaller than 0.5 mm), and consequent increase of d_{50} , and k_s (Fig. 6), there is a reduction of the total volume of debris flow. From a content of small particles of 22% to a content of 18%, the simulated volume at the depositional fan decreases from 648,431 m³ to 602,556 m³ (Table 3). With the content decreasing to 16%, 14% and 12%, the volume decrease becomes more pronounced, down to a minimum amount of just 51,511

m^3 . For lower contents of small particles, erosion of the co-seismic deposits does not occur at all in our test conditions. These results reveal the prime control of the small particles content on the hillslope erosion. This is in agreement with the experimental results presented by [Hu et al. \(2017\)](#), who suggested that the small particles play an important role in the initiation and runout of debris flows. In this regard, a high content of small particles may be the key to the generation and the sustainment of large positive pore pressure excess, which is a key contributor to the initiation and runout of debris flow ([Iverson et al., 1997](#)). However, the numerical approach used in this research focuses on the initiation of debris flows by runoff erosion, while it does not account for the generation of pore water pressures directly. Thus, it cannot offer an explicit simulation of the internal instability phenomena triggered by the reduction of the available shear strength upon reduction of suction, saturation and generation of positive pore water pressures ([Fredlund and Rahardjo, 1993](#)). The decreasing of the small soil fraction, and the consequent increasing of d_{50} and k_s is translated into a reduction of i (eq. 4) and of h_r (eq. 6). Conceptually, the increase of k_s hinders the generation of excess of rain and the consequent runoff with sufficient capacity of erosion. On the other hand, the larger the d_{50} the higher the energy (runoff) necessary to destabilize the sediment layer is. In terms of time, the rate at which the grain coarsening proceeds should mostly depend on the rain and on the debris flow events that wash away the smaller particles. In this research, the d_{50} corresponding to the exhaustion of fine particles is 3.5 mm. According to the observations made by [Zhang et al. \(2014\)](#) in the Pubugou Ravine, this mean grain size is in the range between the debris flow occurred in 2008 and 2010 suggesting that: 1) the washing away of fine particles in the Wenchuan earthquake-affected area is a rapid process that might be completed in less than two years, and 2) this process produces an increase of the critical rainfall thresholds after this period of time ([Guo et al., 2016a](#); [Yu et al., 2014](#); [Zhou and Tang, 2014](#)).

Table 3. d_{50} and k_s used for each small particle content (dimension smaller than 0.5 mm) (Fig. 5). The resulting simulated volume at the depositional fan is shown.

| Small particle content (%) | d_{50} (mm) | k_s (m/h) | Volume of depositional fan (m^3) |
|----------------------------|---------------|-------------|--------------------------------------|
| 22 | 1.9 | 0.003 | 648,431 |
| 18 | 2.3 | 0.003 | 602,556 |
| 16 | 2.4 | 0.004 | 447,907 |
| 14 | 2.5 | 0.005 | 289,602 |
| 12 | 2.7 | 0.007 | 51,511 |
| 9 | 2.9 | 0.008 | 0 |
| 6 | 3.1 | 0.009 | 0 |
| 4 | 3.2 | 0.010 | 0 |
| 2 | 3.3 | 0.012 | 0 |
| 0 | 3.5 | 0.018 | 0 |

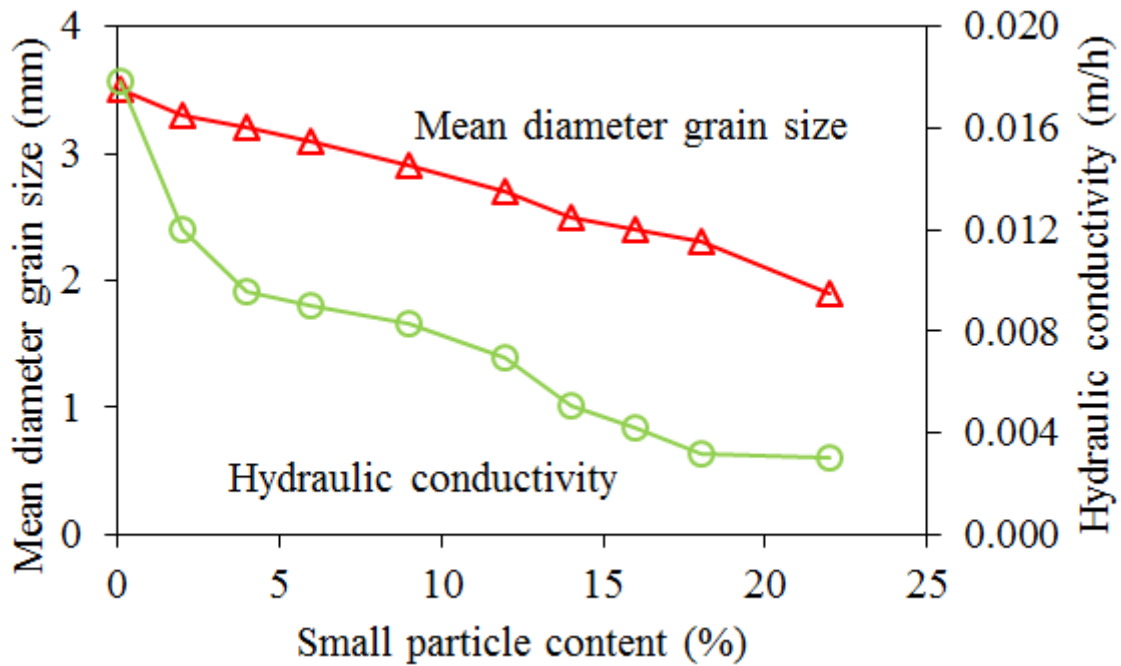


Figure 6. Relationship between the content of small particles (dimension smaller than 0.5 mm), k_s (at a given relative density (Hu et al., 2018)) and d_{50} : this relationship has been used to simulate the effect of the grain coarsening (Fig. 4b).

The effects of the vegetation restoration over time (2010, 2013 and 2015) are shown in [Fig. 4c](#). There is a decrease of the calculated total volume of debris flows. From 2010 to 2013 the decrease is of about 27% which is higher than that from 2013 to 2015 (6%). The reason relies on the higher increment of τ_c and decrease of δ_e from 2010 to 2013 than that from 2013 to 2015 ([Table 4](#)). Nevertheless, the results indicate that although the vegetation restoration is reducing the hillslopes erosion, the calculated debris flow volume is still considerable with 459,765 m³ of material that reach the depositional fan in 2015. This may be related to the fact that the arboreal revegetation is a slow processes and in 2015 the vegetation has not fully recovered to the pre-seismic levels ([Yang et al., 2018](#)). At this point, it is important to stress that these results are based on the values obtained by [Shen et al. \(2017\)](#) in another area which is close to Hongchun gully. Nevertheless, the entire gully may not follow the same history of the study area analysed by [Shen et al. \(2017\)](#) as the revegetation can proceed at different rates depending on terrain conditions such as aspect, slope, soil type, etc. Furthermore, vegetation restoration takes place only where landslide remobilisations no longer occur or slope movements are very low (e.g. creep deformation). In other words, if substantial remobilisations are observed via satellite imagery during the period 2010-2015, these slopes cannot be considered with the same degree of vegetation as the dormant ones during the analysis of 2015. Hence, these results must be taken only as a first approach that indicates the potential of the revegetation in mitigating the hillslope erosion.

Table 4. δ_e and τ_c used to reproduce the effect of the revegetation. The values refer to the co-seismic deposits in the years 2010, 2013 and 2015 according to the *RMD* obtained by [Shen et al. \(2017\)](#). The simulated debris flow at the depositional fan is listed.

| Year | <i>RMD</i> (%) | δ_e | τ_c (kPa) | Volume of depositional fan (m ³) |
|------|----------------|------------|----------------|--|
| 2010 | 0 | 0.10 | 1.0 | 648,431 |
| 2013 | 0.16 | 0.06 | 1.8 | 483,520 |
| 2015 | 0.40 | 0.04 | 2.4 | 459,765 |

In summary, among the three analysed processes, grain coarsening of the loose deposits is the factor that reduces the hillslope erosion the most, and hence limits the consequent generation of debris flows in the short term (from 2008 to 2015).

4.3 Influence of material depletion, grain coarsening and revegetation on the critical rainfall thresholds

The changes on the critical rainfall threshold as a consequence of material depletion, grain coarsening and vegetation restoration have been calculated by a power law (Fig. 7):

$$I = \alpha D^{-\beta} \quad (18)$$

where I (mm/h) is the intensity of a rainfall event of a duration D (h) from the beginning until the occurrence of the debris flow and α and β are constants.

The curves have been built by interpolating simulated rainfall events, with a given intensity and duration, and considering whether they produced a debris flow at the depositional fan or not. The effect of the antecedent rainfall has not been considered in the analysis directly: it can influence the initial moisture content, especially for the short and intense events just before the triggering rain (some hours to 1 day), and thus the critical threshold curves (van Asch et al., 2014). Furthermore, the antecedent rainfall does not play an important role for high intensity rains triggering debris flow by runoff. Additionally, the antecedent rainfall that occurred in Hongchun gully within the last 24 hours preceding the debris flow was relatively small (see Fig. 1).

The changes on the critical rainfall threshold as a consequence of the material depletion are shown in [Fig. 7a](#). There is a shift of the ID curve after two simulations due to the depletion of material in the main channels. However, for the further simulations, the critical rainfall to generate sufficient runoff for a given runout distance until the outlet of the catchment cannot be calculated because of the lack of material to be eroded. After four simulations, the exhaustion of most of this material prevents the generation of debris flow until the depositional fan. As mentioned earlier, this effect is partly a consequence of the limitations of the code as a strong erosion at the toe of the co-seismic landslides at the main channels would lead to their collapse bringing additional material for the next events.

Conversely, the effects of the grain coarsening on the rainfall thresholds are much more evident ([Fig. 7b](#)). As expected, the critical rainfall threshold increases with the decreasing of the content of small particles. In other words, the fines of the co-seismic deposits are washed away, over time, and the rainfall necessary to generate sufficient runoff increases. From 22% to 2% of small particle content, we observe a gradual increase of the critical rainfall threshold. This increase is even more accentuated between 2% and 0.1%. This large increase, which relates to the corresponding large increase of k_s ([Fig 6](#)), reveals that the runoff erosion is very sensitive to small changes of the small particles content where this content is very low.

For the revegetation of the co-seismic deposits, the evolution of the ID curve is shown in [Fig. 7c](#). The lowest critical rainfall threshold is given for the bare ground case (2010) and it increases as the vegetation colonises the loose deposits in 2013 (mid-level revegetation) and 2015 (high-level revegetation). This increment is more evident from 2010 to 2013 where the differences between δ_e and τ_c are more significant than between 2013 and 2015. On the one hand, the period from 2010 to 2013 comprises one year more than the 2013-2015, thus the time allowed for the vegetation to recover is longer. On the other hand, in the revegetation analysis carried out by [Yang et al. \(2018\)](#) in the Wenchuan earthquake-affected area from 2008 to 2015,

the vegetation recovery trend tends to slow down for the years 2014 and 2015, which would agree with the lower increment of the critical rainfall threshold in 2015.

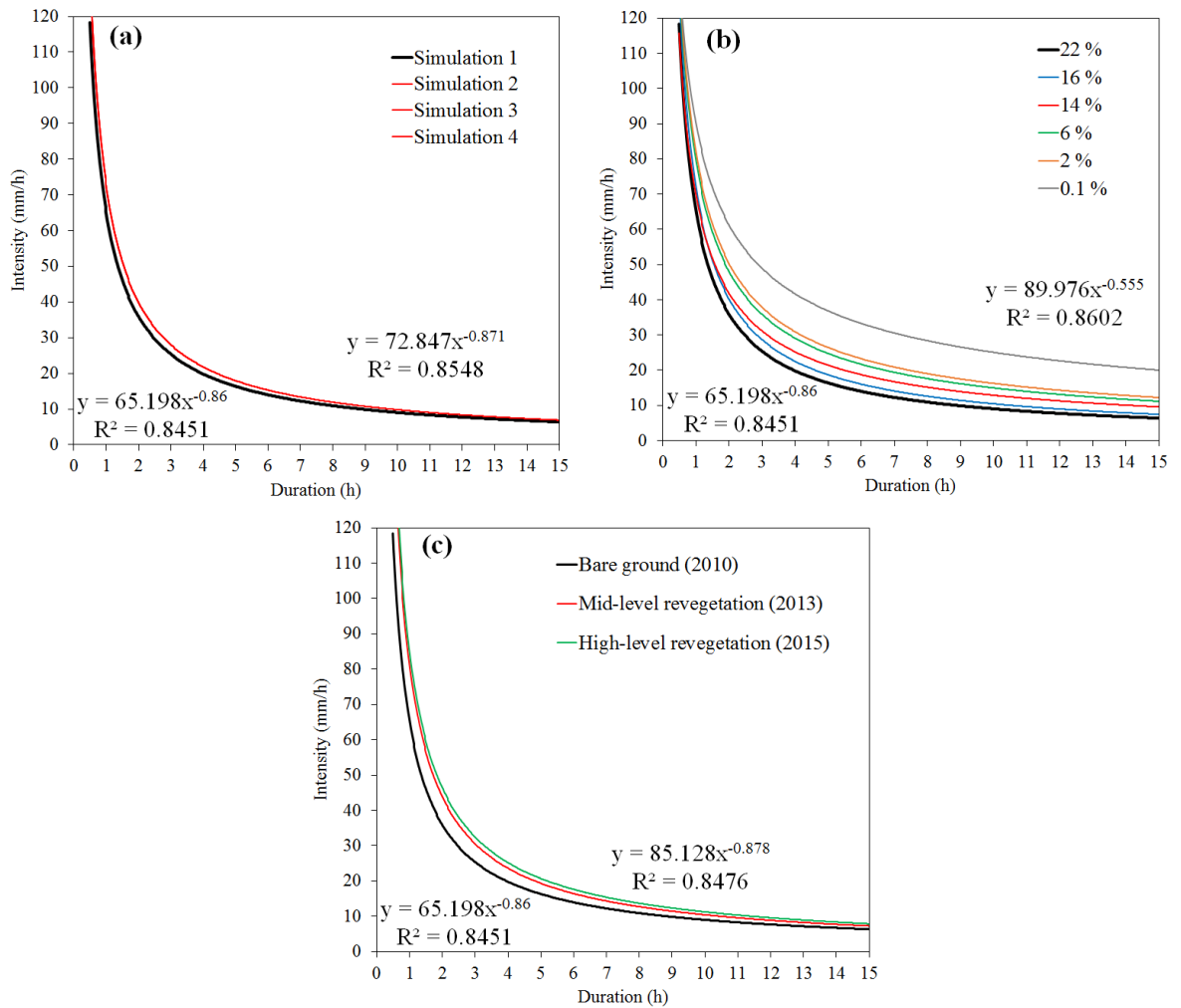


Figure 7. Evolution of the rainfall thresholds for debris flows with deposition at the outlet of Hongchun gully as a consequence of: (a) material depletion of the co-seismic deposits; (b) grain size coarsening of the co-seismic deposits. The grain size evolution has been quantified in terms of percentage of small particle content (dimension smaller than 0.5 mm) (from 22% to 0.1%); (c) revegetation of the co-seismic deposits. The equation of the best-fitted power law and its coefficient of determination are shown for the lowest and highest rainfall threshold of each process.

The values of the ID threshold constant α (eq. 18) found for the three analysed parameters range from 65 to 90 and β from -0.86 to -0.555. They fit with those calculated by [van Asch et al. \(2014\)](#) in Wenjia ($\alpha = 62$; $\beta = -0.705$) and Shuida gullies ($\alpha = 83$; $\beta = -0.71$) during the events that occurred between September 2008 and 2010, and during August 2010, respectively. Conversely, α values are much higher than the ones obtained by other authors at regional scale indicating that the mean rainfall intensity required is higher. Exponent values, which define the variation of the rainfall intensity threshold towards higher rainfall durations, remain in the same order of magnitude: [Guo et al. \(2016b\)](#) found that the threshold increased annually from $I = 5.46D^{-0.75}$ in 2008 to $I = 17.14D^{-0.75}$ in 2013 for rainfall durations of 1 to 135 h after analysing data for 252 rainfall-induced debris flows in the Wenchuan earthquake-affected area. The upper limit of rainfall conditions that did not trigger debris flows was determined as $I = 45.91D^{-0.63}$. [Guo et al. \(2016b\)](#) proposed an ID threshold for the Wenchuan earthquake-affected area as $I = 4.2D^{-0.62}$ ($2 \text{ h} < D < 56 \text{ h}$) for the post-earthquake debris flow events and $I = 11.8D^{-0.87}$ ($2 \text{ h} < D < 56 \text{ h}$) for debris flow during the period of 2009-2013. On the other hand, [Ma et al. \(2017\)](#) obtained $I = 41D^{-0.33}$ for Dujiangyan and $I = 15.2D^{-0.8}$ and $I = 26D^{-0.7}$ for Yingxiu. In contrast with the study presented here and the one performed by [van Asch et al. \(2014\)](#), which correspond to two large events with large triggering rainfalls, the ID thresholds calculated at regional scale are usually defined by the lowest triggering rainfall ([Guo et al., 2016b](#)) being mandatory the smallest debris flow events that require the smallest amount of rainfall. Furthermore, due to the high temporal and spatial variability of rainfalls in mountainous areas, it is difficult to determine the exact triggering rainfall event, which is commonly underestimated ([Abancó et al., 2016](#); [Nikolopoulos et al., 2014](#)).

5. Discussion and conclusion

We used an improved version of the code written by [van Asch et al. \(2014\)](#) in PCRaster environmental modelling language ([Karssenbergh et al., 2001](#)) to analyse the influence of material depletion, grain coarsening and revegetation of the co-seismic deposits on the triggering condition and characteristics of runoff-generated debris flows. We calibrated the model on the 14th August 2010 debris flow event that occurred in Hongchun gully and ran it parametrically in the same catchment.

Grain coarsening has been found to be the most limiting factor for the generation of debris flows, as progressive grain coarsening and the related increase of hydraulic conductivity produce a significant increase of the critical rainfall thresholds. Field observations suggested that the wash-away of the finest soil fraction can be a rather quick process that occurs over just a few years ([Zhang et al., 2014](#)) and during a few consecutive debris flows occurring in the same area. This hinders the generation of additional debris flows even though most of the co-seismic debris remains in place. On the other hand, our quantification of the influence of the material depletion might be biased by the abundance of co-seismic debris in the selected study area. It also might be underestimated because of limitations of the code, which lacks the modelling of sediment supply from further slope instabilities and entrainment of bed material. Revegetation of the co-seismic deposits seems to have a little influence on debris flow occurrence in the short term, as large increases in soil strength seem only achievable by extensive root systems that take several years to develop. However, it also influences hydraulic properties of the soil, and this was not accounted for in this study.

The modelling approach is affected by several limitations, some of which are intrinsic to the simplified nature of numerical approaches in general. The initiation of debris flow by runoff is an underlying hypothesis of the study, made to limit the number of variables and focus

on the relative importance of the investigated processes. Obviously, initiation by runoff is not granted in other areas and in time, as it depends on the nature and state of the debris and bed material, its degree of saturation, its water retention behaviour, and its (evolving) hydraulic conductivity (Cuomo and Della Sala, 2013). Moreover, the relatively small size of the study area, including only one catchment, challenges the representativeness of the results for the much wider Wenchuan earthquake-affected region. However, it is apparent that the modelling approach, regarded as a conceptual, parametric, virtual experiment has been able to identify and rank the first-order controls on the post-earthquake evolution of runoff-generated debris flow occurrence and characteristics in a way consistent with observations and with experimental results from the literature. The approach can be considered as a prototype study to be expanded and improved in studies targeting larger areas and aimed at providing usable insight in post-earthquake debris flow hazard assessments.

Acknowledgments

This research is financially supported by the Fund for International Cooperation (NSFC-RCUK_NERC), Resilience to Earthquake-induced landslide risk in China (grant No. 41661134010), the Funds for Creative Research Groups of China (Grant No. 41521002), National Science Fund for Outstanding Young Scholars of China (Grant No. 41622206). The authors thank the two anonymous reviewers and the editor for their helpful suggestions which helped improve the paper.

References

Abancó, C., Hürlimann, M., 2014. Estimate of the debris-flow entrainment using field and

570 topographical data. *Nat. Hazards* 71, 363–383. doi:10.1007/s11069-013-0930-5

571 Abancó, C., Hürlimann, M., Moya, J., Berenguer, M., 2016. Critical rainfall conditions for the
572 initiation of torrential flows. Results from the Rebaixader catchment (Central Pyrenees).
573 *J. Hydrol.* 541, 218–229. doi:10.1016/j.jhydrol.2016.01.019

574 Chang, D.S., Zhang, L.M., Xu, Y., Huang, R.Q., 2011. Field testing of erodibility of two
575 landslide dams triggered by the 12 May Wenchuan earthquake. *Landslides* 8, 321–332.
576 doi:10.1007/s10346-011-0256-x

577 Chen, H., Dadson, S., Chi, Y.G., 2006. Recent rainfall-induced landslides and debris flow in
578 northern Taiwan. *Geomorphology* 77, 112–125. doi:10.1016/j.geomorph.2006.01.002

579 Chen, H.X., Zhang, L.M., 2015. EDDA 1.0: Integrated simulation of debris flow erosion,
580 deposition and property changes. *Geosci. Model Dev.* 8, 829–844. doi:10.5194/gmd-8-
581 829-2015

582 Chen, H.X., Zhang, L.M., Zhang, S., 2014. Evolution of debris flow properties and physical
583 interactions in debris-flow mixtures in the Wenchuan earthquake zone. *Eng. Geol.* 182,
584 136–147. doi:10.1016/j.enggeo.2014.08.004

585 Cuomo, S., Della Sala, M., 2013. Rainfall-induced infiltration, runoff and failure in steep
586 unsaturated shallow soil deposits. *Eng. Geol.* 162, 118–127.
587 doi:10.1016/j.enggeo.2013.05.010

588 Cuomo, S., Della Sala, M., Novità, A., 2015. Physically based modelling of soil erosion
589 induced by rainfall in small mountain basins. *Geomorphology* 243, 106–115.
590 doi:10.1016/j.geomorph.2015.04.019

591 Cuomo, S., Pastor, M., Capobianco, V., Cascini, L., 2016. Modelling the space–time evolution
592 of bed entrainment for flow-like landslides. *Eng. Geol.* 212, 10–20.
593 doi:10.1016/j.enggeo.2016.07.011

594 De Roo, A.P.J., 1996. The LISEM project: an introduction. *Hydrol. Process.* 10, 1021–1025.

595 Domènech, G., Yang, F., Guo, X., Fan, X., Scaringi, G., Dai, L., Huang, R., 2018. Two multi-
596 temporal datasets to track the enhanced landsliding after the 2008 Wenchuan earthquake
597 (Version V2) [Data set]. Zenodo. doi:doi.org/10.5281/zenodo.1484667

598 Fan, X., Domènech, G., Scaringi, G., Huang, R., Xu, Q., Hales, T.C., Dai, L., Yang, Q., Francis,
599 O., 2018a. Spatio-temporal evolution of mass wasting after the 2008 Mw 7 . 9 Wenchuan
600 Earthquake revealed by a detailed multi-temporal inventory. *Landslides* 1–17.
601 doi:10.1007/s10346-018-1054-5

602 Fan, X., Juang, C.H., Wasowski, J., Huang, R., Xu, Q., Scaringi, G., van Westen, C.J., Havenith,
603 H.B., 2018b. What we have learned from the 2008 Wenchuan Earthquake and its
604 aftermath: A decade of research and challenges. *Eng. Geol.* 241, 25–32.
605 doi:10.1016/j.enggeo.2018.05.004

606 Fan, X., Scaringi, G., Yang, F., Domènech, G., Guo, X., Dai, L., He, C., Xu, Q., Huang, R.,
607 2018c. Two multi-temporal datasets to track the enhanced landsliding after the 2008
608 Wenchuan earthquake. *Earth Syst. Sci. Data Discuss.* 1–29. doi:doi.org/10.5194/essd-
609 2018-105

610 Fredlund, D.G., Rahardjo, H., 1993. *Soil Mechanics for Unsaturated Soils*. John Wiley and
611 Sons, New York. doi:10.1002/9780470172759

612 Guo, X., Cui, P., Li, Y., Fan, J., Yan, Y., Ge, Y., 2016a. Temporal differentiation of rainfall
613 thresholds for debris flows in Wenchuan earthquake-affected areas. *Environ. Earth Sci.*
614 75, 1–12. doi:10.1007/s12665-015-5031-1

615 Guo, X., Cui, P., Li, Y., Ma, L., Ge, Y., Mahoney, W.B., 2016b. Intensity-duration threshold
616 of rainfall-triggered debris flows in the Wenchuan Earthquake affected area, China.
617 *Geomorphology* 253, 208–216. doi:10.1016/j.geomorph.2015.10.009

618 Hales, T.C., 2018. Modelling biome-scale root reinforcement and slope stability. *Earth Surf.*
619 *Process. Landforms.* doi:10.1002/esp.4381

620 Hovius, N., Meunier, P., Ching-weei, L., Hongey, C., Yue-gau, C., Dadson, S., Ming-jame, H.,
621 Lines, M., 2011. Prolonged seismically induced erosion and the mass balance of a large
622 earthquake ☆. *Earth Planet. Sci. Lett.* 304, 347–355. doi:10.1016/j.epsl.2011.02.005

623 Hu, W., Dong, X.J., Xu, Q., Wang, G.H., van Asch, T.W.J., Hicher, P.Y., 2016. Initiation
624 processes for run-off generated debris flows in the Wenchuan earthquake area of China.
625 *Geomorphology* 253, 468–477. doi:10.1016/j.geomorph.2015.10.024

626 Hu, W., Scaringi, G., Xu, Q., Huang, R., 2018. Internal erosion controls failure and runout of
627 loose granular deposits : Evidence from flume tests and implications for post - seismic
628 slope healing 5518–5527. doi:10.1029/2018GL078030

629 Hu, W., Scaringi, G., Xu, Q., Pei, Z., Van Asch, T.W.J., Hicher, P.Y., 2017. Sensitivity of the
630 initiation and runout of flowslides in loose granular deposits to the content of small
631 particles: An insight from flume tests. *Eng. Geol.* 231, 34–44.
632 doi:10.1016/j.enggeo.2017.10.001

633 Huang, R., Fan, X., 2013. The landslide story. *Nat. Geosci.* 6, 325–326. doi:10.1038/ngeo1806

634 Iverson, R.M., Reid, M.E., LaHusen, R.G., 1997. Debris-flow mobilization from landslides.
635 *Annu. Rev. Earth Planet. Sci.* 25, 85–138. doi:10.1146/annurev.earth.25.1.85

636 Julian, J.P., Torres, R., 2006. Hydraulic erosion of cohesive riverbanks. *Geomorphology* 76,
637 193–206. doi:10.1016/j.geomorph.2005.11.003

638 Karssenberg, D., Karssenberg, D., Burrough, P. a., Burrough, P. a., Sluiter, R., Sluiter, R., de
639 Jong, K., de Jong, K., 2001. The PCRaster Software and Course Materials for Teaching
640 Numerical Modelling in the Environmental Sciences. *Trans. GIS* 5, 99–110.
641 doi:10.1111/1467-9671.00070

642 Kean, J.W., McCoy, S.W., Tucker, G.E., Staley, D.M., Coe, J.A., 2013. Runoff-generated
643 debris flows: Observations and modeling of surge initiation, magnitude, and frequency. *J.*
644 *Geophys. Res. Earth Surf.* 118, 2190–2207. doi:10.1002/jgrf.20148

645 Li, D., Xu, X., Ji, F., Cao, N., 2013. Engineering management and its effect of large debris
646 flow at Hongchun valley in Yingxiu town. Wenchuan Country. *J. Eng. Geol.* 21, 260–268
647 (in Chinese).

648 Ma, C., Wang, Y., Hu, K., Du, C., Yang, W., 2017. Rainfall intensity–duration threshold and
649 erosion competence of debris flows in four areas affected by the 2008 Wenchuan
650 earthquake. *Geomorphology* 282, 85–95. doi:10.1016/j.geomorph.2017.01.012

651 Mamo, M., Bubenzer, G.D., 2001. Detachment rate, soil erodibility, and soil strength as
652 influenced by living plant roots. Part I: laboratory study. *Trans. Am. Soc. Civ. Eng.* 44,
653 1167–1174. doi:10.13031/2013.6445

654 Marc, O., Hovius, N., Meunier, P., Uchida, T., Hayashi, S., 2015. Transient changes of
655 landslide rates after earthquakes. *Geology* 43, 883–886. doi:10.1130/G36961.1

656 Montgomery, D.R., Buffington, J.M., 1997. Channel-reach morphology in mountain drainage
657 basins. *GSA* 109, 596–612. doi:10.1130/0016-
658 7606(1997)109<0596:CRMIMD>2.3.CO;2

659 Morgan, R.P.C., Quinton, J.N., Smith, R.E., Govers, G., Poesen, J.W.A., Auerswald, K., Chisci,
660 G., Torri, D., Styczen, M.E., 1998. The European Soil Erosion Model (EUROSEM): a
661 dynamic approach for predicting sediment transport from fields and small catchments.
662 *Earth Surf. Process. Landf.* 23, 527–544.

663 Nearing, M.A., Foster, G.R., Lane, L.J., Finkner, S.C., 1989. A process-based soil erosion
664 model for USDA–Water Erosion Prediction Project technology. *Trans. ASAE* 32, 1587–
665 1593.

666 Nikolopoulos, E.I., Crema, S., Marchi, L., Marra, F., Guzzetti, F., Borga, M., 2014. Impact of
667 uncertainty in rainfall estimation on the identification of rainfall thresholds for debris flow
668 occurrence. *Geomorphology* 221, 286–297. doi:10.1016/j.geomorph.2014.06.015

669 Ouyang, C., He, S., Tang, C., 2015. Numerical analysis of dynamics of debris flow over
670 erodible beds in Wenchuan earthquake-induced area. *Eng. Geol.* 194, 62–72.
671 doi:10.1016/j.enggeo.2014.07.012

672 Reubens, B., Poesen, J., Danjon, F., Geudens, G., Muys, B., 2007. The role of fine and coarse
673 roots in shallow slope stability and soil erosion control with a focus on root system
674 architecture: a review. *Trees* 21, 385–402. doi:10.1007/s00468-007-0132-4

675 Saito, H., Korup, O., Uchida, T., Hayashi, S., Oguchi, T., 2014. Rainfall conditions, typhoon
676 frequency, and contemporary landslide erosion in Japan. *Geology* 42, 999–1002.
677 doi:10.1130/G35680.1

678 Schwarz, M., Cohen, D., Or, D., 2010. Root-soil mechanical interactions during pullout and
679 failure of root bundles. *J. Geophys. Res. Earth Surf.* 115, 1–19.
680 doi:10.1029/2009JF001603

681 Shen, P., Zhang, L.M., Chen, H.X., Gao, L., 2017. Role of vegetation restoration in mitigating
682 hillslope erosion and debris flows. *Eng. Geol.* 216, 122–133.
683 doi:10.1016/j.enggeo.2016.11.019

684 Takahashi, T., Nakagawa, H., Harada, T., Yamashiki, Y., 1992. Routing debris flows with
685 particle segregation. *J. Hydraul. Eng.* 118, 1490–1507. doi:10.1061/(ASCE)0733-
686 9429(1992)118:11(1490)

687 Tang, C., Zhu, J., Ding, J., Cui, X., Chen, L., Zhang, J., 2011. Catastrophic debris flows
688 triggered by a 14 August 2010 rainfall at the epicenter of the Wenchuan earthquake.
689 *Landslides* 8, 485–497. doi:10.1007/s10346-011-0269-5

- van Asch, T.W.J., Tang, C., Alkema, D., Zhu, J., Zhou, W., 2014. An integrated model to assess critical rainfall thresholds for run-out distances of debris flows. *Nat. Hazards* 70, 299–311. doi:10.1007/s11069-013-0810-z
- Veylon, G., Ghestem, M., Stokes, A., Bernard, A., 2015. Quantification of mechanical and hydric components of soil reinforcement by plant roots. *Can. Geotech. J.* 52, 1839–1849. doi:https://doi.org/10.1139/cgj-2014-0090
- Waldron, L.J., Dakkessian, S., 1981. Soil reinforcement by roots: calculation of increased soil shear resistance from root properties. *Soil Sci.* 132, 427–435. doi:10.1097/00010694-198112000-00007
- Wang, G., Sassa, K., 2003. Pore-pressure generation and movement of rainfall-induced landslides: effects of grain size and fine-particle content. *Eng. Geol.* 69, 109–125. doi:http://dx.doi.org/10.1016/S0013-7952(02)00268-5.
- Wang, G., Sassa, K., 2001. Factors affecting rainfall induced flowslides in laboratory flume tests. *Géotechnique* 51, 587–599. doi:10.1680/geot.2001.51.7. 587
- Wang, W., Godard, V., Liu-Zeng, J., Scherler, D., Xu, C., Zhang, J., Xie, K., Bellier, O., Ansberque, C., de Sigoyer, J., 2017. Perturbation of fluvial sediment fluxes following the 2008 Wenchuan earthquake. *Earth Surf. Process. Landforms* 42, 2611–2622. doi:10.1002/esp.4210
- Weiler, M., McDonnell, J., 2004. Virtual experiments: A new approach for improving process conceptualization in hillslope hydrology. *J. Hydrol.* 285, 3–18. doi:10.1016/S0022-1694(03)00271-3
- Weiler, M., McDonnell, J.J., 2006. Testing nutrient flushing hypotheses at the hillslope scale: A virtual experiment approach. *J. Hydrol.* 319, 339–356. doi:10.1016/j.jhydrol.2005.06.040

714 Wu, T.H., 2013. Root reinforcement of soil: review of analytical models, test results, and
 715 applications to design. *Can. Geotech. J.* 50, 259–274. doi:10.1139/cgj-2012-016

716 Yang, W., Qi, W., Zhou, J., 2018. Decreased post-seismic landslides linked to vegetation
 717 recovery after the 2008 Wenchuan earthquake. *Ecol. Indic.* 89, 438–444.
 718 doi:10.1016/j.ecolind.2017.12.006

719 Yu, B., Wu, Y., Chu, S., 2014. Preliminary study of the effect of earthquakes on the rainfall
 720 threshold of debris flows. *Eng. Geol.* 182, 130–135. doi:10.1016/j.enggeo.2014.04.007

721 Zhang, G., Tang, K., Ren, Z., Zhabg, X.C., 2013. Impact of grass root mass density on soil
 722 detachment capacity by concentrated flow on steep slopes. *Trans. Am. Soc. Agric. Biol.*
 723 *Eng.* 56, 927–934. doi:10.13031/trans.56.9566

724 Zhang, S., Zhang, L.M., 2017. Impact of the 2008 Wenchuan earthquake in China on
 725 subsequent long-term debris flow activities in the epicentral area. *Geomorphology* 276,
 726 86–103. doi:10.1016/j.geomorph.2016.10.009

727 Zhang, S., Zhang, L.M., Chen, H.X., 2014. Relationships among three repeated large-scale
 728 debris flows at Pubugou Ravine in the Wenchuan earthquake zone. *Can. Geotech. J.* 51,
 729 951–965. doi:10.1139/cgj-2013-0368

730 Zhang, S., Zhang, L.M., Chen, H.X., Yuan, Q., Pan, H., 2013. Changes in runout distances of
 731 debris flows over time in the Wenchuan earthquake zone. *J. Mt. Sci.* 10, 281–292.
 732 doi:10.1007/s11629-012-2506-y

733 Zhou, W., Tang, C., 2014. Rainfall thresholds for debris flow initiation in the Wenchuan
 734 earthquake-stricken area, southwestern China. *Landslides* 11, 877–887.
 735 doi:10.1007/s10346-013-0421-5

736 Zhu, H., Zhang, L.M., 2016. Field investigation of erosion resistance of common grass species
 737 for soil bioengineering in Hong Kong. *Acta Geotech.* 11, 1047–1059.

738 [doi:10.1007/s11440-015-0408-6](https://doi.org/10.1007/s11440-015-0408-6)

739